

Light scattering by lungs correlates with stereological measurements

SHUNSUKE SUZUKI, JAMES P. BUTLER, EBEN H. OLDMIXON, AND
FREDERIC G. HOPPIN, JR.

*The Memorial Hospital and Brown University, Pawtucket, Rhode Island 02860; and
Harvard School of Public Health, Boston, Massachusetts 02115*

SUSUKI, SHUNSUKE, JAMES P. BUTLER, EBEN H. OLDMIXON, AND FREDERIC G. HOPPIN, JR. *Light scattering by lungs correlates with stereological measurements.* J. Appl. Physiol. 58(1): 97-104, 1985.—The pattern of light backscattered by lung tissue should depend strongly on the size of air spaces and equivalently on the internal surface area of the lung. To verify and apply this, we shone a laser beam into excised lungs through the pleural surface and measured the backscattered light surrounding the beam with a focused photodetector. The intensity, I , fell off as a function of distance, r , from the point of entry of light. The configurations of $I(r)$ curves corresponded closely to theory over a 3-decade range of I . $I(r)$ changed systematically with lung volume. The optical mean free path, λ , was calculated from $I(r)$ curves in a series of canine lobes fixed immediately after optical scanning and was compared with stereological measurement of mean linear intercept, L_m , an index of alveolar size. At high lung volumes the relation of λ to L_m was consistent with reflection by alveolar septa. At lower lung volumes there appeared to be, additionally, a substantial refractive component. This technique is independent of current stereological methods and has the advantages of being noninvasive, continuous, and potentially applicable to dynamic events in unfixed lungs.

mean linear intercept; surface-to-volume ratio; light scattering; stereology of the lung; air space dimensions

at the internal configuration of the lung in unfixed specimens.

We had initially considered direct visualization of subpleural structures through the pleural surface (4, 13) and rejected it because of concern that light reflection and refraction would compromise quantitative measurements at sufficient depth to be representative of average alveoli. The idea then suddenly occurred to one of us (*JPB*) that these very properties could be put to effective use, that the pattern of light backscattered by reflection and refraction within the parenchyma might yield to analysis, as has been done for light scattered by fog or clouds (3), in terms of the mean distances between the scattering bodies. In a cloud the bodies are water particles. In the lung the scattering bodies would be the alveolar surfaces. The idea was attractive to us because the mean distance between alveolar septa, L_m , is a prime stereological parameter characterizing the size of air spaces and the amount of alveolar surface area per unit volume, S/V . These are measurements of physiological importance to gas exchange and to issues of micromechanics of the lung, such as the nature of the interaction between surface tension and the solid structures.

Our pilot experiments immediately confirmed that the glow returning from the lung when a beam of light is shone into the pleural surface changes dramatically with lung volume. We then set out to characterize this behavior theoretically and experimentally. The theory of how reflection, refraction, and absorption should affect light scattering and of how to recover the relevant parameters from the light-scattering measurements is presented in a companion paper (2). Here we report careful measurements of light scattering in excised lungs and compare them with the theoretical predictions and with stereological measurements in lungs which we fixed immediately after light scattering. Along the way we encountered difficulty in preparing lungs for stereology by standard techniques. We now attribute the difficulty to inadequate mechanical fixation of elastin. This problem and what we believe is an advance towards the elusive goal of preserving the geometry of elastic structures in the lung is presented in another companion paper (14).

On the basis of these studies we believe that light scattering in the lung is strongly dependent on the mean distance between alveolar septa and also on their prism-like configuration. The pattern of light scattering should

CLASSIC CONCEPTS of the mechanics of the lung at the level of alveoli and alveolar ducts have relied on inferences drawn from volume-pressure behavior of the lung, the known properties of the lung's connective tissue, and air-liquid surfaces, and simple models of lung structure. Recent advances have been made by the recognition of the complexity of the relevant structural geometry (6, 10, 12, 15) and by the use of stereological techniques on fixed tissues for measuring the effects on the alveolar surface configuration of changes in lung volume (5, 7, 8, 11) and of changes in the state of the air-liquid interface (1, 7). However, there are limitations inherent in using fixed tissues. These include 1) the restriction to analyses of static circumstances, 2) the difficulties of being certain that no changes occur during the various processes which assail the tissue between the original physiological condition and its fixed, dehydrated, sliced, and stained state, and 3) the necessity of studying a specimen from a different lobe or animal to obtain each individual physiological datum. We sought a means, therefore, of looking

provide stereological information on unfixed lungs by an independent, noninvasive, and continuous method.

METHODS

Lung preparation. Fifteen mongrel dogs (weight 14.1 ± 1.4 kg) were anesthetized with intravenous pentobarbital sodium (35 mg/kg) and then given heparin (5,000 U) and papaverine (60 mg) intravenously to prevent contraction of vascular smooth muscle. An endotracheal tube was inserted and ventilation maintained with a small animal respirator (Harvard Apparatus 615). The thorax was opened bilaterally by intercostal incision and sternal transection. The pericardium was opened and two catheters (ID 0.115 in.) were inserted through the right ventricular outflow tract into the left and right lower branches of the pulmonary artery. The great vessels were then severed in the abdomen. The ties around the catheters were immediately drawn tight, and perfusion was started from a reservoir 15–20 cm above the hilum. The initial perfusate was lactated Ringer solution (3% dextran; bubbled with 100% O₂; pH 7.4; osmolarity 365 mosM). The left atrium was opened. After the surfaces of the perfused lobes became white, the lung and heart were removed en bloc from the chest and both lower lobes were dissected. During dissection the lobes were perfused continuously. After dissection the lobes were drained briefly and weighed to determine tissue volume, with the assumption of a specific gravity of 1.07. A bronchial cannula and a catheter for the pulmonary vein were inserted.

The total volume of the lobe was determined by measuring buoyancy in saline. Air volume was calculated by subtraction of tissue volume. The lobe was then connected to an inflation apparatus consisting of an air column displaced by water driven by a nonperistaltic pump (Fluid Metering RP-D). Occasional air leaks were obvious from the pressure-volume behavior of the lobe, in particular as pressure losses during the several minutes of the light-scattering measurements or as volume losses shown by direct measurements of lung dimensions (14). These lobes were discarded. While the light-scattering measurements and fixation were being done in the first lobe, the second lobe was perfused continuously.

Perfusion fluids were circulated at flow rates of 90–125 ml/min by a nonperistaltic pump with an air trap. Perfusates were 37°C. Initially the lung was inflated to 30 cmH₂O until atelectasis was no longer apparent on the pleural surface. Differential pressure transducers (Validyne MP45) were used to record the volume of gas displaced into the lung (as the change in the product of the cross-sectional area and differential pressure across the water column), the inflating pressure of the lung, the pulmonary arterial pressure relative to airway pressure, and pulmonary venous pressure. The lobe weight was monitored by suspending the perfused lung system from a force displacement transducer (Grass FT.03) except during the light-scattering measurements when mechanical stability was important. After the lobe weight became stable, several inflation-deflation maneuvers between 30 and 3 cmH₂O were performed at flow rates of up to 400 ml/min. The pressure-volume loop for the last maneuver

was recorded X-Y (Hewlett-Packard 4075 A). V₃₀ was defined as the absolute air volume at 30-cmH₂O distending pressure.

Light measurements. The lung was mounted to permit light-scattering measurements, vascular perfusion, and volume-pressure cycling as shown schematically in Fig. 1. The light source was a He neon laser (Airotech LSR5P) with a wavelength of 632.8 nm and output 5 mW. The beam was focused on one end of a plastic optical fiber (diam 0.75 mm) with both ends sheathed in 19G needles to secure their positions. The tips of the fiber were rounded by heat to get better light transmission and prevent damage to the lobe. The incident light was brought to the surface of the lobe by the distal end of the optic fiber. The lobe was hung vertically, and the dorsolateral surface, which is relatively flat, was gently touched to a vertical Plexiglas plate with a vertical slit 0.6×3.0 cm. The light intensity measured at the pleural surface was not very sensitive to small changes of the force with which the lung touched the plate. The tip of the optic fiber was in the same plane as the surface of the Plexiglas plate and was oriented normal to the plane of the plate in the upper third of the center of the slit.

Measurement of the light emanating from the pleural surface was made by a photodetector. A cylinder (ID 1.0 cm, length 12.5 cm) held a lens, three baffles, a pinhole, and the photodetector. The convex lens (focal length 5.0 cm), mounted on the end of the cylinder, focused the light on the pinhole. The three baffles were placed at equal intervals between the lens and the pinhole to prevent reillumination. The position of the pinhole was 10 cm from the lens, and the light detector was located just behind the pinhole. Because the active area of the light detector was not small (5.1 mm²) and we wanted to measure a sharply restricted field, we used a pinhole with a diameter of 1.0 mm. The photodetector was a silicone photodiode (EG&G HUV-1000B) with an integral field effect transistor operational amplifier which had a linearity within 1% over 5 decades (manufacturer's specifications). The range of light intensity in the present study was 3 decades. The optics were focused to measure a circular area of ~1.0-mm diameter on the surface of the lobe 10 cm away from the lens. Figure 2 shows the sharp response to the system as it passed across an illuminated hair of ~60- μ m diameter. The optical axis was normal to the lobe surface. It could be moved vertically, parallel to the lobe surface, by a micromanipulator, and its position was recorded by a linear differential transformer (Hewlett-Packard Linearsyn 5890T-2000 B4). Light intensity, I , and the position of the detector assembly relative to the point of light entry, r , were recorded X-Y (Hewlett-Packard 4075 A).

The structures inside the cylinder, the supporting plate, and other surrounding structures were painted black to prevent reillumination. The laser, both ends of the optic fiber, and the detector were firmly fixed to the optical bench. The optical bench was mounted on a thick aluminum plate ($48 \times 18 \times \frac{3}{4}$ in.) which was isolated from mechanical noise with pneumatic vibration isolators. Before each experiment the horizontal orientation of the detector was set by rotating it horizontally at the level of the light source to find the local valley of intensity

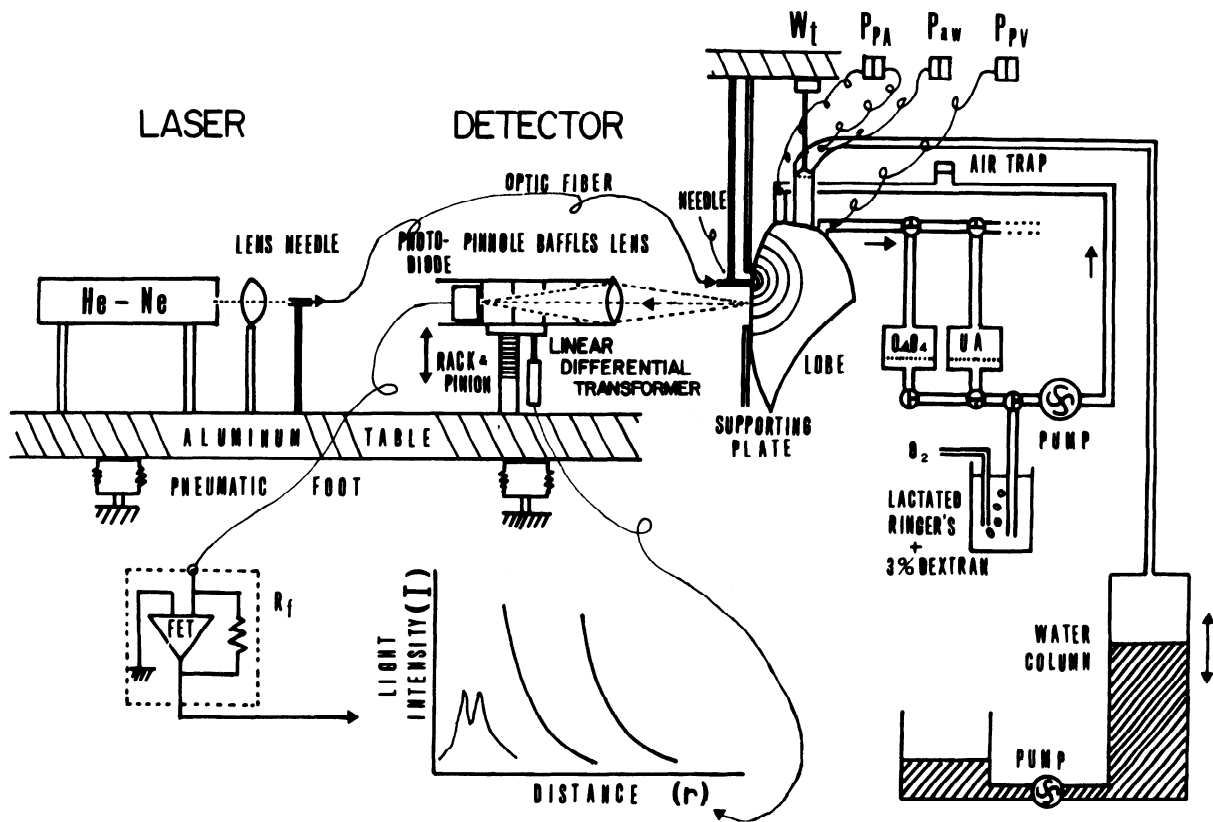


FIG. 1. A schematic diagram of experimental setup. On left is shown laser and optic fiber which brings a beam of light onto pleural surface and photodetector system which records intensity, I , of light backscattered from lobe as a function of distance, r , from point of entry of light.

On right are shown setup for perfusion with lactated Ringer, fixing or dehydrating fluids, and setups for weighing, inflating, and deflating lobe.

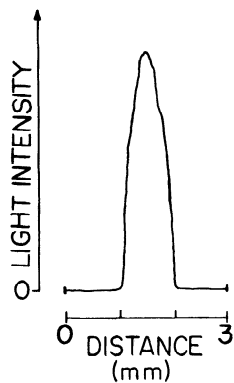


FIG. 2. A tracing of light intensity against position showing response of optical system to an illuminated hair of $\sim 60\text{-}\mu\text{m}$ diameter. Field of view is 1-mm diameter.

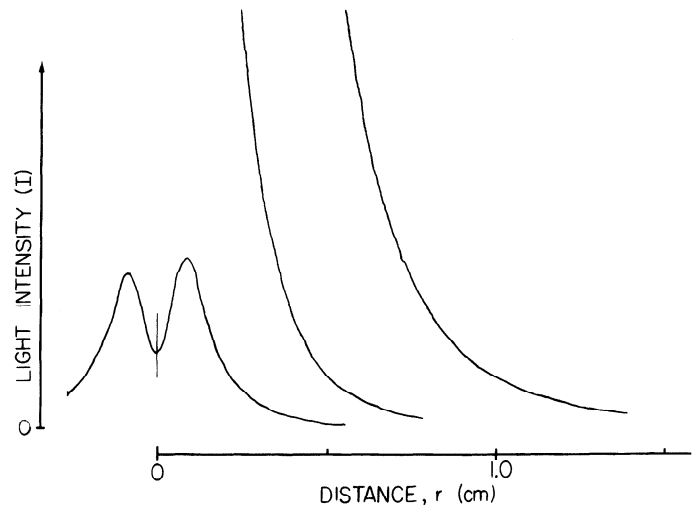


FIG. 3. Direct tracing of light intensity, I , as a function of distance from point of entry of light, r . Left hand tracing shows a valley which represents shadow of needle holding optic fiber establishing location of $r = 0$. Other curves show fall of I over 3 decades. Amplification is increased in nominally 10-fold steps with each of subsequent curves.

caused by the black needle which held the light source. The light-measuring system was then run on a standard piece of fine polyurethane foam fixed in the place of the lung. Over a period of 5 mo of experiments the configurations of the I vs. r curves made on this standard remained undetectably different, while the amplitude of I varied by $<5\%$. No drift could be detected in the system over a period of minutes.

To record the tracings over more than 3 decades of I , the gain of the photodiode/op amp unit was changed in nominally 10-fold steps and the position of the detector was backtracked to overlap the curves at each gain. This overlap established the exact gain (Fig. 3). The curves

were then digitized (Summagraphics digitizing tablet Bit Pad One). To handle the 3 decades of variation in I and to facilitate comparison with theory, the product $I \cdot r^3$ was plotted semilogarithmically against r (Fig. 4). The characterization of these curves in terms of the optical mean free path, λ , and effective extinction coefficient, k , is detailed in the companion paper (2).

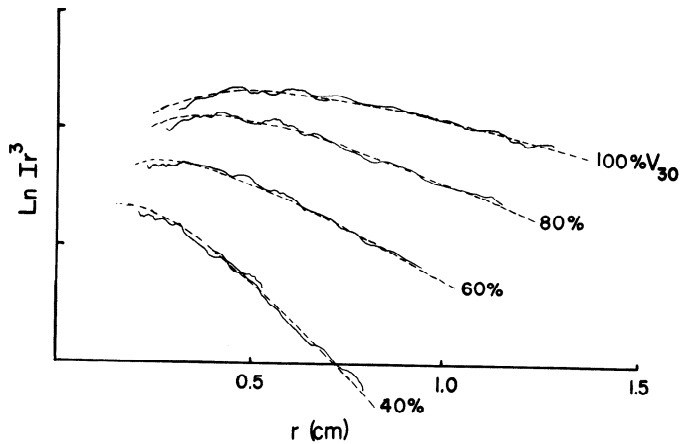


FIG. 4. $\ln Ir^3$ vs. r at 4 different volumes in a single lobe. Experimental data are shown as solid lines; two segments obtained at different gains as in Fig. 3 are fitted by computer for optimal overlap. Dotted lines show theoretical curves generated by computer for best-fit values of mean free path (λ) and effective extinction coefficient (k). Note close correlation of experimental and theoretically derived curves. Note also increase in intensity and decrease of slope with increasing lung volume. I , intensity; r , distance from point of entry of light.

Light-scattering measurements were made in seven lobes during stepwise inflation-deflation maneuvers to 100, 80, 6, and 40% V_{30} . In 17 lobes, light-scattering measurements were made at one of these % V_{30} after deflation from 100% V_{30} and were immediately followed by intravascular perfusion for fixation and dehydration. The perfusion fixation and subsequent stereological analyses are described in the companion paper (14).

RESULTS

The light intensity, I , leaving the lung fell off as a function of the distance, r , from the point of entry of light over the range 0.25–1.3 cm (Fig. 3).

Repeated tracings were reproducible often to within the pen's width. Comparisons of tracings obtained on the same lung at the same lung volume after similar volume gains showed much less difference than the difference in tracings at different lung volumes. Similarly, tracings obtained after shifting the site of light entry by 1 or 2 cm showed relatively small differences as long as we stayed on the relatively flat pleural surfaces away from

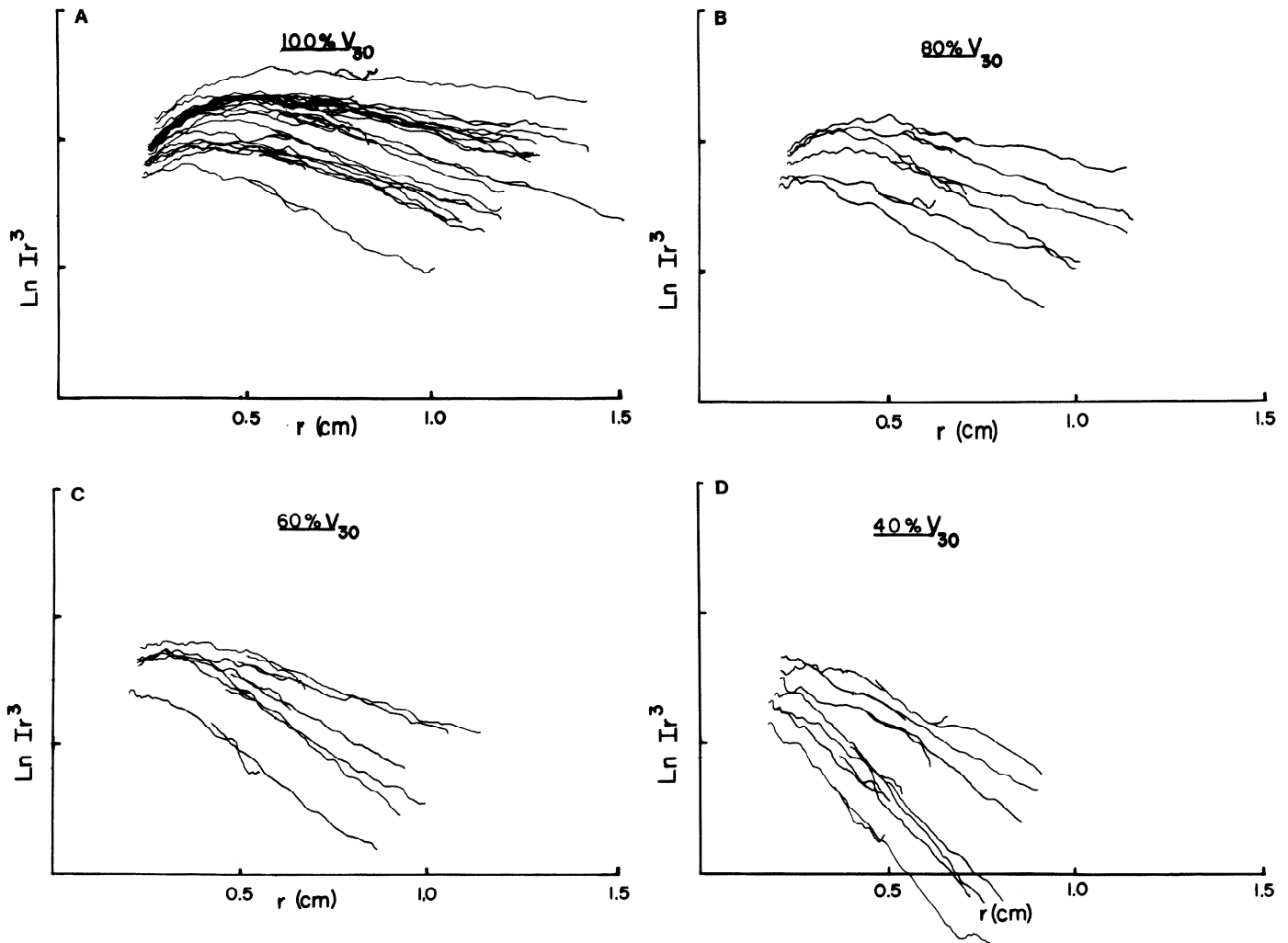


FIG. 5. Tracings (similar to that of Fig. 4) showing $\ln Ir^3$ as functions of distance obtained at 4 lung volumes. All data in 10 animals whose lungs were fixed are shown. I , intensity; r , distance from point of entry of light; V_{30} , absolute air volume at 30-cmH₂O distending pressure.

lobar margins. There were occasional humps on the tracings deviating by <10% from a smooth curve over 1 mm. We thought that these probably represented the presence of a relatively large bronchovascular structure near the pleura. These several observations convinced us that the tracings were reliable and reproducible and that the light-scattering properties of the subjacent lung were relatively insensitive to the exact location.

The continuous curves in Fig. 4 show typical $\ln I r^3$ vs. r plots for a single lung at four different volumes. At each volume, $\ln I r^3$ increases briefly then falls off nearly linearly with the distance.

The dashed curves in Fig. 4 are generated by Eq. 8 in the accompanying theoretical paper (2) which predicts the distance-dependency of light intensity. This is a function of the mean free path of photons and the extinction coefficient, a parameter primarily dependent on the absorption of light by lung tissue. The values for these parameters were ascertained for a given experimental curve by a best-fit process with least mean-squared residuals. The average residuals over all runs ($n = 99$) were 3.8%. Inspection shows a close fit of the theoretical to the experimental curves.

The patterns of light intensity are strongly dependent on lung volume (Fig. 4); at higher lung volumes back-scattered light was much more intense and fell off with distance much less rapidly. There is scatter in the results among animals at a given % V_{30} (Fig. 5) but the differences at different % V_{30} are generally greater. In any given animal, however, the shift in $I(r)$ with lung volume always followed the pattern shown in Fig. 4. λ has a strong correlation with % V_{30} (Fig. 6); at higher lung volumes photons travel farther before being scattered.

Values of k showed considerable variability and no particularly systematic relation to lung volume. The product λk represents the probability of a scattering event being absorptive (2). The average value of λk over

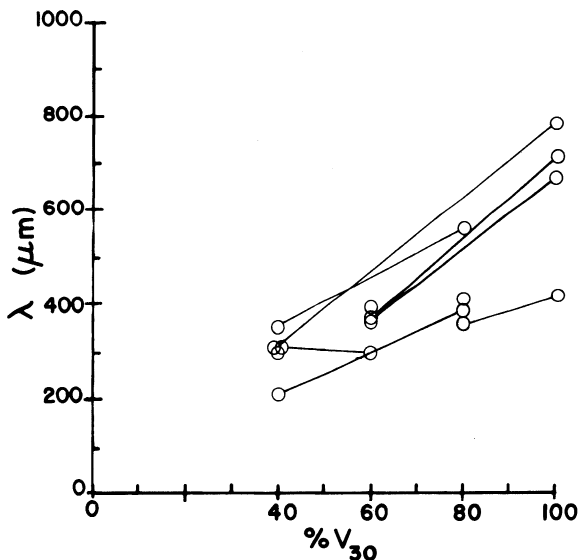


FIG. 6. Mean free path, λ , calculated from light-scattering data plotted against lung volume at which light-scattering measurements were made, absolute air volume at 30-cmH₂O distending pressure (% V_{30}) in 17 dog lobes. Paired data from different lobes in a given animal are connected.

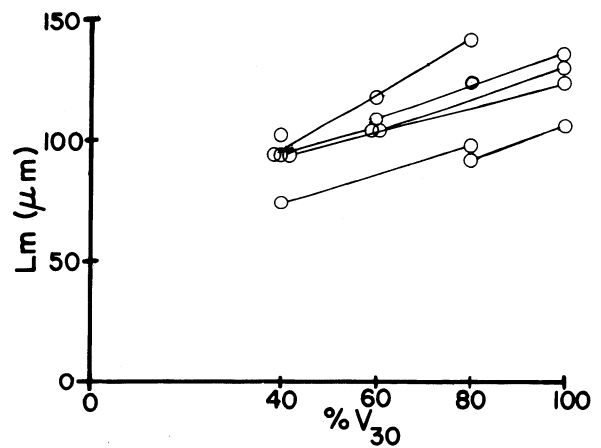


FIG. 7. Comparison of morphometric parameter, L_m , with absolute air volume at 30-cmH₂O distending pressure, % V_{30} , in 17 dog lobes. Paired data from different lobes in a given animal are connected by thin lines.

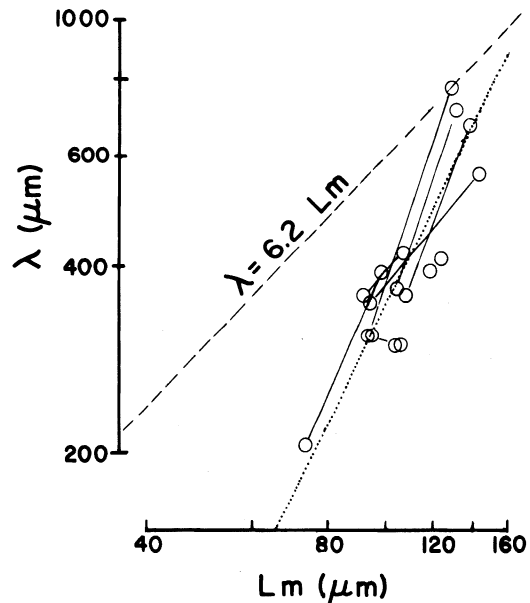


FIG. 8. Comparison of optical and stereological results in 17 dog lobes. Mean free path, λ , is shown plotted against L_m , mean distance between septa. Line $\lambda = 6.2 L_m$ provides an estimate of mean distance between alveolar septa assuming a predominantly reflective mechanism of light scattering. Note correspondence of experimental and theoretical values at high lung volumes. At lower lung volumes optical λ is shorter implying an additional mechanism of scattering. Dotted line shows a best-fit estimate of optical and stereological relationship.¹

all runs was 0.0076 ± 0.0044 . While the effect of absorption on the shape of the $I(r)$ curves may not be negligible, this low value implies that absorption has a negligible effect on λ .

Stereology on lobes prepared by intravascular fixation and dehydration gives values for the mean distance between septa. There is again a strong volume dependency (Fig. 7). There is considerable scatter, confirming the findings of others (1, 5, 7, 8). However, data from paired lobes from a given animal, designated by thin lines in

¹ The dotted line is a two-stage best fit: first, the paired data were used to get a best slope; subsequently all data were used, given that slope, to get a best-fit line.

Figs. 6 and 7, show relatively consistent changes with volume. This suggests that a part of the scatter in alveolar size at a given volume is attributable to the differences among animals.

We expected from the theory that the distance between alveolar surfaces would be a major determinant of the mean free path. This would appear to be the case (Fig. 8).

DISCUSSION

We were able to make satisfactory measurements of the light-scattering properties of excised dog lobes. Measurements of light intensity as a function of distance from the point of light entry, $I(r)$, were reproducible and were highly characteristic of a given lung volume in a series of lobes (Figs. 4 and 5). The theoretical basis for interpreting the pattern of backscattered light, adapted to the lung from knowledge about light scattering in clouds, is developed in the companion paper (2). Four experimental findings give strong support to the validity of this theory as applied to the lung.

First, the distance dependency of backscattered light intensity fits theoretical predictions. We expected the theory to hold at distances greater than several optical mean free paths from the point of entry. Our measurements were made beyond $r = 0.25$ cm which represents $\sim 4 \lambda$ at V_{30} ranging to 8λ at $40\% V_{30}$. We were able to get good measurements from this point out to between 0.8 and 1.3 cm from the point of origin where the light intensity had fallen off by more than 2 decades. The shape of these experimental curves over this enormous range of intensity was closely matched by the theory (Fig. 4).

Second, the absolute intensity of light is compatible with estimates based on the theory. The APPENDIX outlines a backcalculation of the incident photon intensity based on the observed $I(r)$ and the characteristics of the photodiode, the electronics, and the optics. This results in an estimate of 5.7 mW in striking agreement with the laser's nominal output of 5 mW. This photon accounting is an independent test of the validity of the theory as applied to the lung.

Third, the optical mean free paths calculated from the observed curves using the light-scattering theory are reasonable in absolute magnitude and in changes of magnitude with inflation and deflation. Photons passing through the lung are scattered by reflection off alveolar surfaces, by refraction as they pass through septa with nonparallel surfaces, and by light absorption. The contribution of reflection is shown in Fig. 8 as the dashed line. This constitutes an upper bound on the optical mean free path for that L_m (or that surface-to-volume ratio). The extent to which the septal surfaces are parallel is the extent to which the mean free path and L_m ought to be related by the approximate factor 6.2 (obtained by assuming a septal refractive index equal to that of water).

Finally, there is a favorable comparison of optical and stereological results (Fig. 8). We cannot claim that this is the ultimate validation of the light-scattering technique because with any method of preparation of lung

tissue for microscopic studies there is a degree of uncertainty, as discussed in the second companion paper (14), that the precise original shape and dimensions at the level of the alveolar surfaces are retained. Nonetheless favorable comparisons between two totally independent approaches substantially increase confidence in both.

At high lung volumes the coincidence of the optical upper bound on mean interseptal distances with stereological measurements is tight but at lower lung volumes the optical estimates systematically depart from the reflective bound. This implies an additional mechanism of light scattering. Since tissue absorbency is small, the discrepancy is probably related to light refraction. Inspection of micrographs of lungs fixed at different degrees of inflation show that at high lung volumes the opposing surfaces of a septum are nearly parallel (7). Photons passing through them will not be substantially deflected by refraction. At lower lung volumes, however, septal tissue gathers in the corners of alveoli and pulmonary capillaries bulge from the alveolar surface (7). The resulting nonparallel septal surfaces scatter photons refractively. The increasing departure of $\lambda/6.2$ from L_m , then, at lower lung volumes is consistent with increasing refraction by increasingly nonparallel septal surfaces. At this time we do not know how to separate the effects of refraction from reflection from the light-scattering data themselves.

Using the relationship of λ and L_m in Fig. 8 we can make an optical estimate of the mean linear intercept, $L_{m,opt}$. In seven dog lobes stepwise inflation-deflation maneuvers were performed between 40 and 100% V_{30} and light-scattering measurements were made at each step. We derived λ , used the connection curve of Fig. 8 to obtain $L_{m,opt}$, and plotted $L_{m,opt}$ against lung volume in Fig. 9.

Three observations are of particular note. First, the loops described have a slope of approximately one-third on the log-log plot, consistent with the linear dimensions of the air spaces varying as $VL^{1/3}$ and the alveolar surface area varying as $VL^{2/3}$, as one would expect if the config-

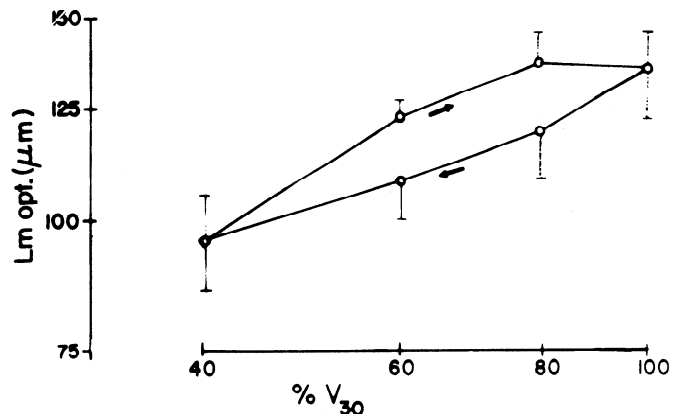


FIG. 9. A plot of alveolar size estimated optically, $L_{m,opt}$, using connection curve of Fig. 8, $L_{m,opt}$, against lung volume during inflation-deflation maneuvers between 40 and 100% of absolute air volume at 30-cmH₂O distending pressure (V_{30}) in 7 dog lobes. Note that overall slope of loop is $\approx 1/3$ implying geometric similarity during volume changes. Note also hysteresis showing longer distances during inflation than during deflation at a given volume.

urations of the alveolar surfaces stayed the same as lung volume changed, that is, if the changes of linear and surface dimensions within the lung were geometrically similar.

Secondly there is hysteresis; at a given volume $L_{m,opt}$ is larger (or, equivalently, the surface-to-volume ratio is smaller) during inflation than during deflation. This implies different configurations of the alveolar surfaces in inflation and deflation. Configuration at this level depends on the mechanical interactions of surface tension with the solid tissue components (9, 15); in particular, surface tension on the alveolar surfaces is mechanically in series with the solid tissue elements of the network of alveolar entrance rings which bounds the alveolar duct. Thus an increase of surface tension at a given lung volume will retract the alveolar septa away from the center of the alveolar duct decreasing their surface areas and dilating the alveolar duct. Our results, which show less surface at a given volume during inflation, are therefore consistent with the surface tension being higher during inflation than during deflation. This is consistent with the effect of the known hysteresis of alveolar surface tension. Hysteresis of the solid tissue elements in the alveolar entrance rings would have the opposite effect. Our results suggest that the effects of surface-tension hysteresis dominate.

Third, the optical intensity at a radial distance r from the source is influenced by the optical properties of the parenchyma at depths up to approximately r . Thus, since our average r is on the order of 1 cm, we may expect that we are sampling lung tissue to depths of ~ 1 cm. In particular, our results are not simply determined by the dimensions of immediately subpleural alveoli.

Two caveats apply to using the connection in Fig. 8. First is the problem inherent in using fixed tissues, namely that there is no absolute assurance that the lung geometry has been precisely preserved (4). The second is the possibility that scattering by refraction may differ at a given lung volume and thus cause the relationship of optical and morphometric measurements to depart from the connection curve of Fig. 8. To the extent that refraction is an important factor in determining λ and to the extent that the nonparallel character of the septal surfaces is not a single-valued function of lung volume, the connection curve could be in error.

Our purpose in this research was to evaluate a possible method for obtaining information about the configuration and dimensions of the lung parenchyma. In its favor the method and its underlying theory are certainly independent of the only other available experimental method, stereology on fixed tissues. It is also noninvasive and can be applied continuously in a given lung, whereas the other methods must use a different lobe for every

datum. Furthermore as the measurements can be obtained continuously the approach may lend itself to dynamic measurements. Our experimental results support the applicability of the theory in the lung. An initial application to interrupted inflation-deflation maneuvers gives results for optical estimates of morphometric parameters which are reasonable in terms of known physiology. The major limitation at this stage of development is our inability to assess the role of refraction.

APPENDIX

The photon flux I is representable (2) as $I_0 F(r, \lambda, k)$, where I_0 is the incident intensity. Further, our fitting procedure compared logarithmically the recorder pen deflection, D , with theoretical prediction, F (taking I_0 to be unity). These were found to have an average logarithmic difference of 4.068. That is, we may write $\langle D \rangle / \langle F \rangle = \exp(4.068) \text{Cm} \cdot \text{cm}^2 = 58.44 \text{Cm} \cdot \text{cm}^2$ where we denote recorder deflection units as Cm, and the units of F are centimeter squared. Now this average deflection may be predicted by

$$\langle D \rangle = I_0 \langle F \rangle \Delta A k_{acc} k_{diode} k_{amp} k_{recorder}$$

where the units of I_0 are Watts, ΔA is the observed area of the pleural surface (cm^2), k_{acc} is the fraction of the photon flux emitted at all angles intercepted by the acceptance lens, k_{diode} is the efficiency of the diode (V/W), k_{amp} is the amplifier factor, and $k_{recorder}$ is the recording scale (Cm/V).

From Fig. 2 the active optical area has diameter 0.1 cm so that $\Delta A = 0.0079 \text{cm}^2$. A lens radius of 0.5 cm at a distance of 10 cm corresponds to a half angle of 0.05, and therefore a solid angle $\Delta\Omega$ of $\pi (0.05)^2 = 0.00785$. Assuming uniform hemispherical flux, this corresponds to a photon fraction $k_{acc} = 0.00785/2\pi = 0.00125$. The diode's quantum efficiency is ~ 6 with an output of 120 MV/W with 200-M Ω feedback (manufacturer's specifications). We used 1-M Ω feedback as our standard so that $k_{diode} = (0.6) (120 \text{MV}/W) (1M\Omega/200 \text{M}\Omega) = 360 \text{kV}/W$. The amplifier was uniformly used at a gain of 400, and the recorder was set at 5.08 Cm/V. Solving the above for I_0 yields $I_0 = 58.44 \text{Cm} \cdot \text{cm}^2 / (0.0079 \text{cm}^2) (0.00125) (360 \text{kV}/W) (400) (5.08 \text{Cm}/V) = 8.1 \text{mW}$. The nominal laser output is 5 mW so that we find not unreasonable agreement in attempting to account for all the photons.

Note that we have explicitly assumed a uniform hemispherical photon flux in calculating the photon fraction k_{acc} subtended by the acceptance lens. Using the Eddington approximation described in the companion paper (2), a more accurate expression is given by $(10/7) \Delta\Omega/2\pi = 0.00179$. Using this value rather than 0.00125 in the above, we get

$$I_{0,Eddington} = 8.1 \text{mW} (0.00125/0.00179) \\ = 5.7 \text{mW}$$

We thank Judy Keller for her careful and cheerful technical work on this project and Dr. Jeffrey C. Smith for many fruitful discussions. We also give particular thanks to Dr. Peter Gehr for his invaluable help, advice, and enthusiasm.

This investigation was supported by National Heart, Lung, and Blood Institute Grants HL-26863 and HL-28797.

Current address of S. Suzuki: First Dept. Internal Medicine, Tohoku University School of Medicine, Sendai, Japan.

Received 12 September 1983; accepted in final form 22 August 1984.

REFERENCES

1. BACHOFEN, H., P. GEHR, AND E. R. WEIBEL. Alterations of mechanical properties and morphology in excised rabbit lungs rinsed with a detergent. *J. Appl. Physiol.* 47: 1002-1010, 1979.
2. BUTLER, J. P., S. SUZUKI, E. H. OLDMIXON, AND F. G. HOPPIN, JR. A theory of diffuse light scattering by lungs. *J. Appl. Physiol.* 58: 89-96, 1985.
3. CHANDRASEKHAR, S. On the diffuse reflection of a pencil of radia-

- tion by a plane-parallel atmosphere. *Proc. Natl. Acad. Sci. USA* 44: 933-940, 1958.
4. FLICKER, E., AND J. LEE. Equilibrium of force of subpleural alveoli: implications to lung mechanics. *J. Appl. Physiol.* 36: 366-374, 1974.
5. FORREST, J. B. The effect of changes in lung volume on the size and shape of alveoli. *J. Physiol. London* 210: 533-547, 1970.
6. FUNG, Y.-C. Stress, deformation, and atelectasis of the lung. *Circ.*

- Res. 37: 481-496, 1975.
7. GIL, J., AND E. R. WEIBEL. Morphological study of pressure-volume hysteresis in rat lungs fixed by vascular perfusion. *Respir. Physiol.* 15: 190-213, 1972.
 8. GIL, J., H. BACHOFEN, P. GEHR, AND E. R. WEIBEL. Alveolar volume-surface area relation in air- and saline-filled lungs fixed by vascular perfusion. *J. Appl. Physiol.* 47: 990-1001, 1979.
 9. HOPPIN, F. G., JR., AND J. HILDEBRANDT. Mechanical properties of the lung. In: *Bioengineering Aspects of the Lung*, edited by J. B. West. New York: Dekker, 1977, vol. 3, p. 83-162. (Lung Biol. Health Dis. Ser.)
 10. KARAKAPLAN, A. D., M. P. BIENIEK, AND R. SKALAK. A mathematical model of lung parenchyma. *J. Biomech. Eng.* 102: 124-136, 1980.
 11. KLINGELE, T. G., AND N. C. STAUB. Alveolar shape changes with volume in isolated, air-filled lobes of cat lung. *J. Appl. Physiol.* 28: 411-414, 1970.
 12. MEAD, J., T. TAKISHIMA, AND D. LEITH. Stress distribution in lungs: a model of pulmonary elasticity. *J. Appl. Physiol.* 28: 596-608, 1970.
 13. MORECAI, A. P., AND J. C. NORMAN. Measurements of alveolar sac diameters by incident light photomicrography. *Am. Thorac. Surg.* 15: 179-186, 1973.
 14. OLDMIXON, E. H., S. SUZUKI, J. P. BUTLER, AND F. G. HOPPIN, JR. Perfusion dehydration fixes elastin and preserves lung air-space dimensions. *J. Appl. Physiol.* 58: 105-113, 1985.
 15. WILSON, T. A. Relations among recoil pressure, surface area, and surface tension in the lung. *J. Appl. Physiol.* 50: 921-926, 1981.

